

Study of the Influence of Nickel Content and Reaction Temperature on Glycerol Steam Reforming with Ni/La₂O₃-SiO₂ Catalysts

Vivian Vazquez Thyssen¹; Francisco Guilherme Esteves Nogueira²; Elisabeth Moreira Assaf^{3*}

^{1,3}(Instituto De Química De São Carlos - Universidade De São Paulo - São Carlos/SP - Brazil)

²(Departamento De Engenharia Química - Universidade Federal De São Carlos - São Carlos/SP - Brazil)

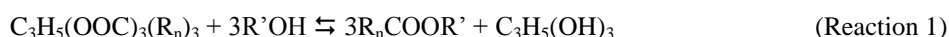
ABSTRACT: La₂O₃-SiO₂-supported nickel catalysts were evaluated in glycerol steam reforming. The samples (30wt% La and 5, 10 and 15wt% of Ni on 70wt% commercial SiO₂), prepared by the simultaneous impregnation method, were characterized by EDX, nitrogen physisorption, XRD, in-situ XRD, XANES and TPR. The analyses revealed NiO species weakly interact with the support and the different metallic surface areas of the catalysts. Catalytic tests were performed in a fixed bed reactor at 600°C and 15Ni catalyst, which showed the best performance, was also evaluated at 500°C and 700°C. According to the results, the Ni content on the catalyst surface interferes in the distribution of gaseous products H₂, CO, CO₂ and CH₄. The increase in the Ni content increases the carbon formation during reaction. The reaction temperature affected the catalytic performance and the best results were obtained with the 15Ni catalyst at 600°C, which was also tested for 20 hours for the analysis of its stability.

Keywords: catalysts; nickel content; steam reforming; glycerol; reaction temperature

I. INTRODUCTION

Most of the world's energy demand is supplied by fossil fuels, which seriously endanger the environment – e.g. increased global warming. Therefore, the use of alternative, clean and sustainable energy sources is vital for the future. The production of H₂ as a fuel has been studied for decades and the most popular methods involve the steam reform of hydrocarbons and alcohols.

Glycerol is produced as a byproduct in the transesterification reaction for the obtaining of biodiesel (Reaction 1), which has been increasingly used as a fuel. Therefore, the extending biodiesel production results in a large supply of glycerol in the market.



The excessive amount of glycerol in the market can be used in the H₂ production, since 1 mol of glycerol can produce 7 mols of H₂ from its steam reforming reaction (Reactions 2-4).



The catalytic conversion of glycerol into H₂, CO₂ and CO involves the preferential cleavage of C-C bonds as opposed to breaking C-O bonds. Studies have suggested catalysts containing Ni favor the breaking of the C-C bond of alcohols for the formation of CH₄, CO₂, CO and H₂. The increase of the Ni content in the catalyst improves such a property. [1-3]

SiO₂ is used as a support in reforming reactions due to its high surface area [4] and La₂O₃ used as an additive is known for its ability to remove the carbon formed during the reaction [3].

Many authors have studied the glycerol steam reforming reaction at different temperatures and observed the conversion of alcohol increases in function of the temperature, whereas the amount of carbon and volume of the liquid effluent collected at the end of the reaction decrease. [5,6]

In previous studies [3,7], we discussed the effect of La₂O₃ content on the support and the effect of the material preparation method. In Thyssen et al. (2013) [3], the best results were achieved with the use of 30wt% La₂O₃ content. Thyssen and Assaf (2014) [7] observed the preparation method of simultaneous impregnation was more effective. Therefore, this paper reports the study of Ni catalysts with different amounts of metal, supported on 30wt%La₂O₃-SiO₂ prepared by simultaneous impregnation, to be used for the obtaining of H₂ from glycerol steam reforming at different temperatures.

II. EXPERIMENTAL

2.1 Preparation

Catalysts were prepared by the simultaneous impregnation method, as described by Thyssen and Assaf (2014) [7], with 5, 10 and 15wt% of Ni deposited on a support composed of 30wt%La₂O₃-70wt%SiO₂ and selected according to Thyssen et al. (2013) [3].

Commercial SiO₂ (Degussa - Aerosil 200) was treated at 600°C for 2h under synthetic air flow. La(NO₃)₃.6H₂O and Ni(NO₃)₂.6H₂O aqueous solutions were simultaneously impregnated in the commercial SiO₂ and calcined at 600°C for 3h, also under synthetic air flow. The catalysts were labeled 5Ni, 10Ni and 15Ni.

2.2 Characterization

Energy-dispersive X-ray (EDX) spectroscopy determined the chemical composition of the catalysts placed under an LEO 440 electron microscope (Leica Zeiss) coupled to an energy-dispersive analyzer (SiLi detector) with a beryllium window (Oxford 7060) and 133eV resolution.

Surface specific areas of the samples were determined by N₂ physisorption (BET method) in a Quantachrome Nova 1000e instrument.

The samples were characterized by X-ray diffraction (XRD) for the identification of the crystalline phases. XRD analyses were performed with CuK α radiation on a Rigaku Multiflex diffractometer. Bragg angle (2 θ) was scanned between 10° and 80° at 2°min⁻¹ and Scherrer's equation (Equation 1) calculated the NiO crystallite size.

$$d_{\text{NiO}} = \frac{\lambda \cdot \sqrt{2}}{\beta \cdot \cos\theta} \quad (\text{Equation 1})$$

where d_{NiO} is the NiO crystallite average size (nm), λ is the incident radiation wavelength (nm), β is the half-height width (radians) of the NiO main peak and θ is the Bragg angle of the peak (°).

XRD analyses were recorded in situ under activation conditions at the Brazilian Synchrotron Light Laboratory-LNLS (Campinas, Brazil) on XPD-10B beamline and in reflection mode, in a 2 θ interval from 40° to 80°, at $\lambda = 1.54996\text{\AA}$ radiation, calibrated with a Si (1 1 1) monochromator. The samples were heated, in situ, under H₂, from 25°C up to the reduction temperature, at 10°Cmin⁻¹, and held at that temperature for 1h. The crystallite size of Ni⁰ (d_{Ni}) was calculated by Equation 1 from in situ XRD patterns.

The metal dispersion of the catalysts (D_{M}) was calculated by Equation 2 from the crystallite size of Ni⁰. The metallic surface area was obtained by Equation 3, where M is the Ni metal atomic weight, N is the Avogadro number and y is the Ni mass fraction assuming a density of active sites on the surface (n_s) 1.54x10¹⁹ Ni atoms.m⁻² [8].

$$D_{\text{M}} = \frac{101.2}{d_{\text{Ni}}} \quad (\text{Equation 2})$$

$$S_{\text{M}} = \frac{D_{\text{M}} \cdot N \cdot y}{n_s \cdot M} \quad (\text{Equation 3})$$

2.3 Catalytic tests

Glycerol steam reforming (GSR) tests were performed as described by Thyssen et al. (2013) [3], at a 3:1 molar water:glycerol ratio, 2.5mLh⁻¹ flow rate and 150mg of catalyst. They were conducted at 600°C for 5h for all catalysts and at 500°C and 700°C for the catalyst with 15wt% of Ni, which was also tested for 20h for the analysis of its stability at 600°C.

Prior to the reaction, the catalysts were activated in situ for 1h under an H₂ flow at 30mLmin⁻¹, at determined TPR temperature profiles (400°C, 600°C and 500°C; for 5Ni, 10Ni and 15Ni, respectively).

The collected effluent was analyzed by gas chromatography in a Shimadzu system with H₂ carrier gas and an HP5 capillary column operating between 35°C and 250°C, with an FID detector. The global glycerol conversion (X_{Glycerol}) was calculated by Equation 4.

$$X_{\text{glycerol}} = \left(\frac{n_{\text{total}} - n_{\text{residual}}}{n_{\text{total}}} \right) \cdot 100 \quad (\text{Equation 4})$$

where n_{total} is the amount of glycerol fed (mol).

A gas chromatograph (Varian GC-3800) was used in-line for the analysis of the gaseous products reaction (H_2 , CO , CO_2 and CH_4). It was equipped with two parallel columns (Porapak-N and Molecular Sieve 13X), with TCD in each of them, operating between 40°C and 80°C , and He and N_2 carrier gases, respectively, at 10mLmin^{-1} . The yield (Y) for the gaseous products was determined according to the ratio of moles of the product formed and moles of the glycerol fed (Equation 5).

$$Y = \frac{\text{mol}_{\text{prod}}}{\text{mol}_{\text{glycerolfed}}} \quad (\text{Equation 5})$$

The qualitative analysis of the accumulated liquid products of the reaction was performed by a GCMS-QP20105 system (Shimadzu) equipped with an rtx-wax column ($30\text{m} \times 1\mu\text{m} \times 0.32\text{mm}$) after the end of the reaction. The column temperature ranged from 40°C to 200°C and a 280°C injector temperature was set.

An EA1110 CHNS-O Elemental Analyzer equipped with a Porapak PQS column determined the carbon formed throughout the reaction.

A scanning electron microscopic (SEM) analysis of the 15Ni catalyst used was performed under an LEO-440 scanning electron microscope equipped with an Oxford detector.

III. RESULTS AND DISCUSSION

3.1 Characterization

The mass compositions of the catalysts, obtained by EDS, are shown in Table 1.

Table 1. Catalysts physicochemical properties.

Catalysts	Content (wt%)		S (m^2g^{-1})	Crystallite size (nm)		TPR- H_2 consumption ($\times 10^{-3}\text{mol}$)	R (%)	D_M (%)	S_M (m^2g^{-1})
	La	Ni		NiO	Ni ⁰				
5Ni	33.1±2.9	4.6±1.2	129	8	34	1.0	7	3	1.0
10Ni	33.5±1.8 ^a	9.8±0.7 ^a	121 ^a	11	20	9.6 ^a	100 ^a	5	3.3
15Ni	31.8±1.6	16.8±1.9	97	13	20	14.1	100	5	5.0

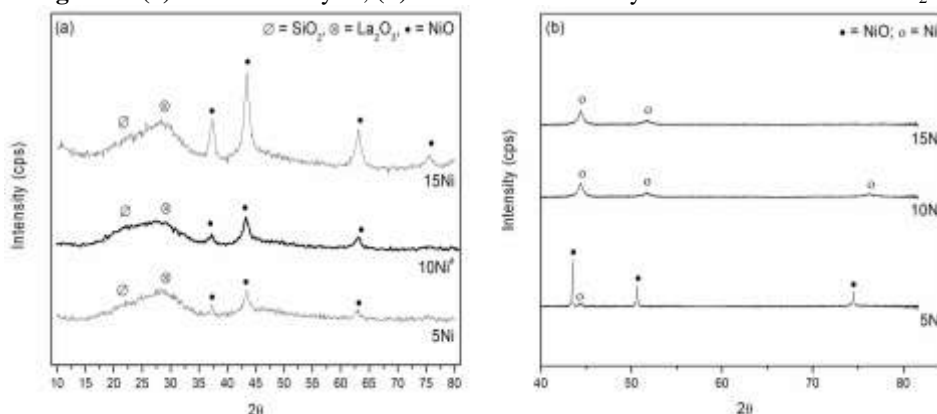
^aData based on Thyssen and Assaf, 2014 [7]

Results for La and Ni were close to those expected, i.e., 30wt% for La(III) and 5, 10 and 15wt% for Ni(II). Slight differences may be due to the manipulation of reagents during the preparation.

Table 1 also shows the BET surface area for catalysts with different Ni(II) contents. According to Guo et al. (2007) [9] and Dieuzeide et al. (2014) [10], the surface area of catalysts with different Ni(II) contents decreases, as the percentage of Ni(II) in the catalyst increases, which was also observed here.

All three catalysts showed the same crystallographic phases in the diffractograms (Figure 1a): besides the structures of the supports, SiO_2 (JCPDS 83-2473) and La_2O_3 (JCPDS 83-1344), only the NiO crystalline phase was observed (JCPDS 78-0643). [3,7]

Figure 1. (a) XRD of catalysts, (b) XRD in situ of catalysts after activation with H_2



^aData based on Thyssen and Assaf, 2014⁷

A low and broad peak is expected for amorphous materials, as they display no regular crystal planes or a long-range structure. [3,7] As shown in Figure 1a, the crystallinity of SiO_2 and La_2O_3 seems to be low.

The difference in the intensity of the NiO peaks may be correlated with the amount of Ni(II) species. An increase in the Ni(II) content of the catalyst increases the intensity of the peaks, which suggests the amount of NiO species is higher in catalysts with a higher Ni(II) content. [11,12]

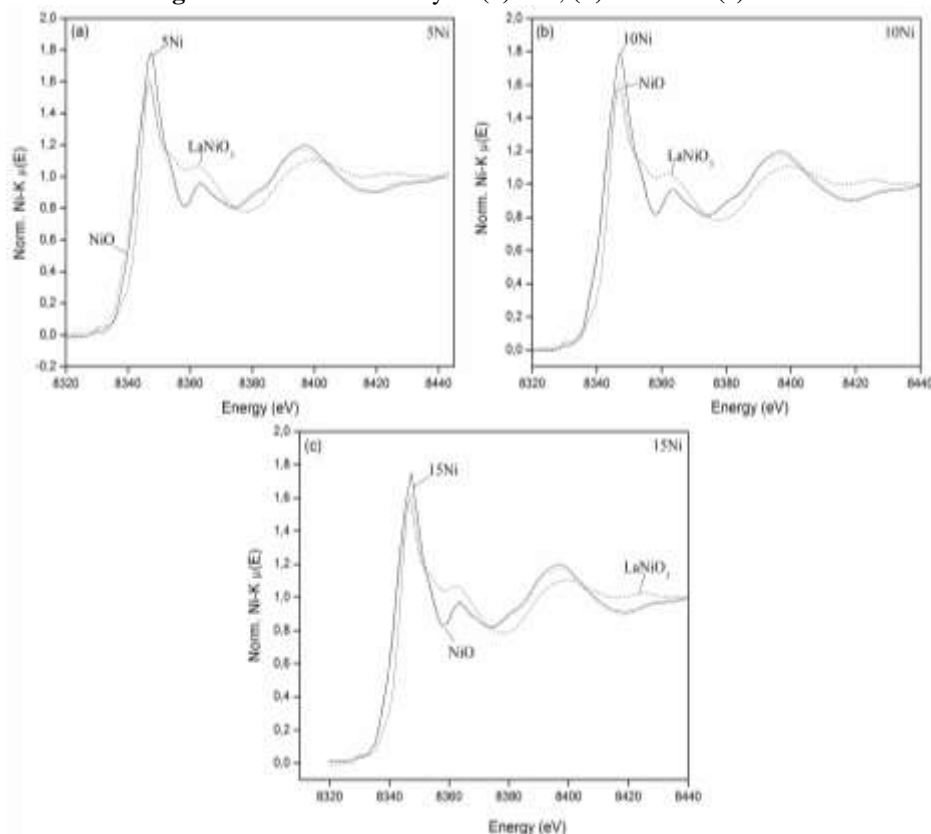
The NiO average crystallite size (Table 1) was estimated by Scherrer's equation (Equation 1) from XRD patterns. It showed a small increase when the Ni(II) content in the catalyst was increased. Li et al. (2012) [13] reported no remarkable NiO particle size change was observed at metal loading below 16wt%.

The in situ XRD (Figure 1b) after the activation process revealed the 10Ni and 15Ni catalysts exhibited only Ni^0 peaks (JCPDS 4-850), whereas 5Ni also showed peaks related to the presence of NiO. The results confirmed the calculus of the reduction degree of the samples (R - Table 1), i.e., all NiO phases in the 10Ni and 15Ni catalysts were reduced to metallic Ni during the reduction process, whereas the 5Ni catalyst showed only a 7% reduction [14]. The Ni^0 average crystallite size is also provided in Table 1.

The metallic dispersion (D_M) of the catalysts (Table 1) was calculated from Ni^0 crystallite size and their metallic areas were calculated from D_M results. Table 1 shows both dispersion and metal areas are larger for smaller Ni^0 crystallite sizes.

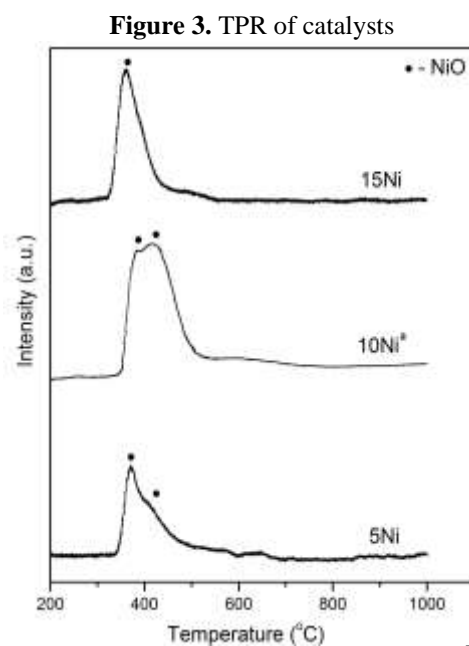
Figure 2 shows the XANES results for the catalysts. The spectral features for all catalysts calcined at 600°C are close to those displayed by the NiO reference spectrum, which leads to the hypothesis the Ni local chemical environment is similar, regardless of the Ni content.

Figure 2. XANES of catalysts (a) 5Ni, (b) 10Ni and (c) 15Ni



The XANES results, along with XRD results, suggest La_2O_3 does not play any meaningful role in the local chemical environment of Ni, which occasionally would form LaNiO_3 wherein Ni would be more strongly interacted with the supporting La_2O_3 , as observed in previous studies [3,7]. Figure 2 shows the LaNiO_3 species are not present in those catalysts.

The TPR profiles of the catalysts are displayed in Figure 3. The catalysts showed a reduction peak around $350\text{-}500^\circ\text{C}$, which represents an Ni-support interaction. According to the XRD results in Figure 1a, the reduction peak in the TPR profiles may be related to the reduction of NiO that weakly interacts with the support. Due to its high mobility on the surface of the material, which leads to an easy migration and possible aggregation of particles, NiO is easily reduced and described as a free state of the Ni active phase, as explained in Thyssen et al. (2013) [3] and Thyssen and Assaf (2014) [7].



The easy migration of NiO particles may explain the low reduction degree of 5Ni (Table 1). Since NiO may be aggregated on the 5Ni surface, its reduction may be difficult.

According to Table 1, the amount of TPR- H_2 consumption increased according to the increase in the Ni(II) content of the catalyst due to the increase in the absolute amount of Ni(II) species. However, such an increase is not proportional to the Ni content, since the amount of Ni in the 5Ni catalyst is much lower than half the amount of 10Ni [15], which may corroborate the aggregation of NiO particles on the 5Ni surface.

In the simultaneous impregnation method, both lanthanum and nickel oxides compete for adsorption sites on silica, as explained in Thyssen and Assaf (2014) [7]. Therefore, for those catalysts, neither a homogeneous surface, nor the presence of Ni(II) species in the bound state are expected – which suggests a stronger interaction with the support. And this may be due to La_2O_3 is not uniformly dispersed over the SiO_2 before the Ni(II) adsorption takes place [7]. The XANES results show La_2O_3 does not play any meaningful role in the local chemical environment of Ni in those catalysts, and since a homogeneous catalyst surface is not expected and NiO is easily aggregated, the NiO reduction is not equal.

3.2 Catalytic tests

Table 2 shows the GSR results for catalysts with different Ni contents.

Table 2. C gaseous product yield ($mol_{prod}/mol_{glycerol\ fed}$), H_2/CO_2 and CO_2/CO rate (mol/mol), volume of liquid effluent collected (mL), global glycerol conversion at 600°C (%) and carbon formation (mmol)

Catalysts	H_2	CH_4	CO	CO_2	H_2/CO_2	CO_2/CO	Effluent	$X_{glycerol}$	C
5Ni	2.0	0.1	0.3	0.7	2.9	2.3	5.8	23	4.0
10Ni ^a	3.8	0.4	1.1	1.5	2.5	1.4	3.8	98	5.0
15Ni	4.6	0.5	1.2	1.8	2.6	1.5	3.3	100	6.0
15Ni - 20h	4.2	0.4	1.0	1.4	2.9	1.4	14.7	100	22.0

^aData based on Thyssen and Assaf, 2014 [7]

The amount of collected liquid is related to the global glycerol conversion, i.e., the higher the amount of the liquid, the lower the global conversion of glycerol reached by the catalyst. The collected effluent was analyzed and acetic acid, propanoic acid, formic acid, ethanol, 2-propanone, propylene glycol, glycidol, 1,3-dioxane and sorbitol were identified.

Metallic Ni is the active phase for GSR to take place, which favors the breaking of the C-C bond. Therefore, the more dispersed the Ni (or the higher the metal surface area), the more active the catalyst. 15Ni catalyst showed the highest activity in the GSR and the largest metallic area.

The catalyst with lowest nickel content (5Ni) showed low GSR activity, which might be explained by the effect of the low metallic area. The products expected during the reaction (H_2 , CH_4 , CO and CO_2) showed

low yield in comparison with the other two catalysts (Figure 4) and also a low global conversion of glycerol. Since the small amount of converted glycerol was not efficiently converted to the expected gaseous product, it would not be efficient for the process.

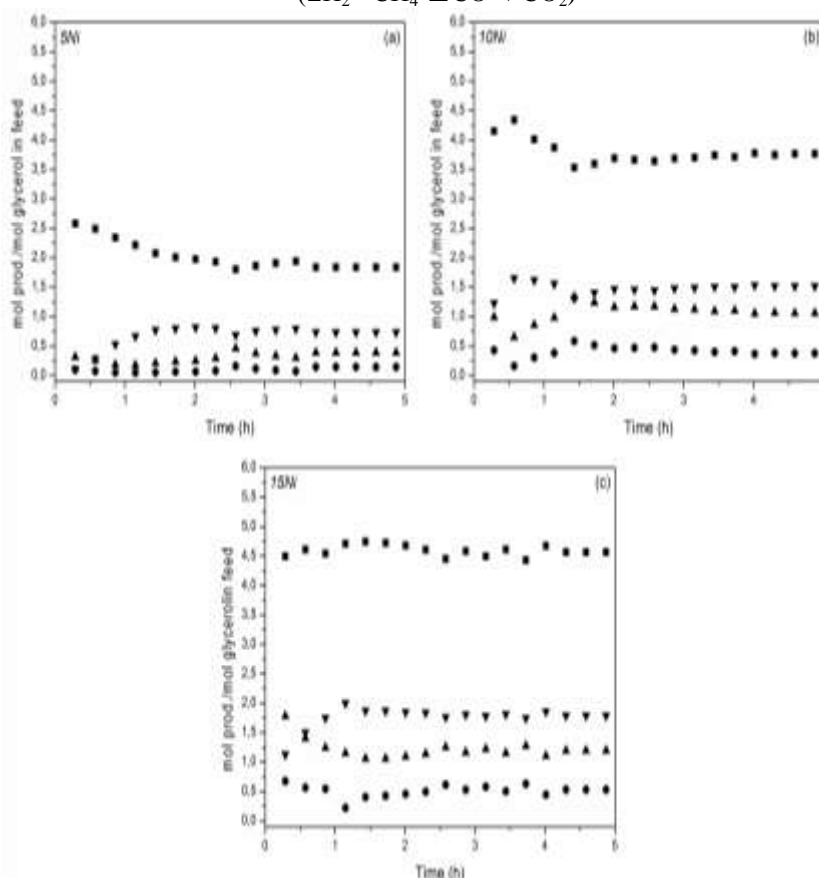
By GSR reaction (Reaction 4), the theoretical H_2/CO_2 ratio is approximately 2.3mol/mol. The ideal value for the CO_2/CO ratio is 1mol/mol, since the shift reaction (Reaction 3), in which the CO formed during the reaction is converted to CO_2 and H_2 , shows an equilibrium and would lead to 1mol/mol CO_2/CO . According to Table 2, the H_2/CO_2 ratio of the three catalysts was larger or very close to the theoretical one (2.3mol/mol) and the CO_2/CO ratio was larger than the theoretical one (1mol/mol), which shows a higher selectivity for CO_2 than for CO in those catalysts.

10Ni and 15Ni catalysts yielded very similar carbonaceous gaseous products (CH_4 , CO and CO_2 – Table 2) – only the H_2 yield showed an improvement with the increase in the Ni content – and both catalysts were active and stable over the entire reaction (Figure 4).

The amount of carbon produced showed a small difference among the catalysts (Table 2) with a slight increase in function of the increase in the Ni content.

The literature [16,17] reports catalysts with Ni as an active phase promoting the formation of carbon as filament, i.e., carbon is deposited between the metal and the supporting surface and forms a filament that can be broken, which results in the deactivation of the catalyst with the loss of the active phase.

Figure 4. GSR of (a) 5Ni, (b) 10Ni and (c) 15Ni
(■ H_2 ● CH_4 ▲CO ▼ CO_2)



The dissociation reaction of CH_4 (Reaction 5) and Boudouard reaction (Reaction 6) may be responsible for the formation of carbon during the catalytic test.



The Boudouard reaction (Reaction 6) should be considered over Ni catalysts, since the presence of nickel species in the form of crystallites – observed in the catalyst characterization – favors the carbon atom diffusion [18]. The increase in the Ni content may increase the amount of Ni on the material surface, therefore, an increase in the carbon deposition at the end of the reaction is also expected.

Despite such a slight increase in the carbon formation with the increase in the Ni content, the 15Ni catalyst showed an excellent H₂ yield and 100% glycerol conversion and its 20-h stability test (Table 2 and Figure 5) showed it was stable and active during all process.

The carbon formation for the 15Ni (Table 2) catalyst was equivalent regarding time, since the carbon deposition rate for the catalyst was 1.1mmolh⁻¹ in a 20-h reaction and 1.2mmolh⁻¹ in a 5-h reaction.

Figure 5. GSR of 15Ni at 600°C for 20h
(■H₂ ●CH₄ ▲CO ▼CO₂)

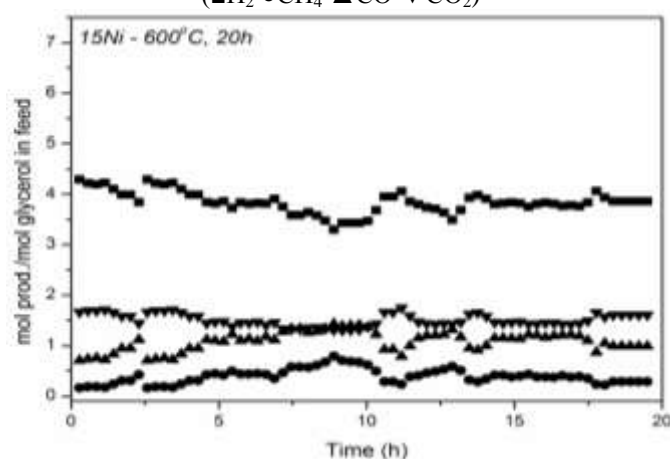


Figure 6 shows the SEM image of the 15Ni catalyst after a 20-h stability test at 600°C and the formation of filamentous carbon over the reaction, as expected. [19-21]

Figure 6. SEM of 15Ni after GSR

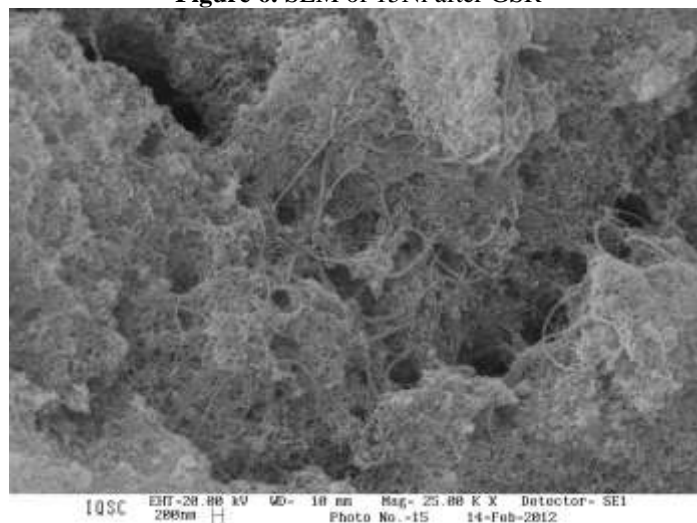
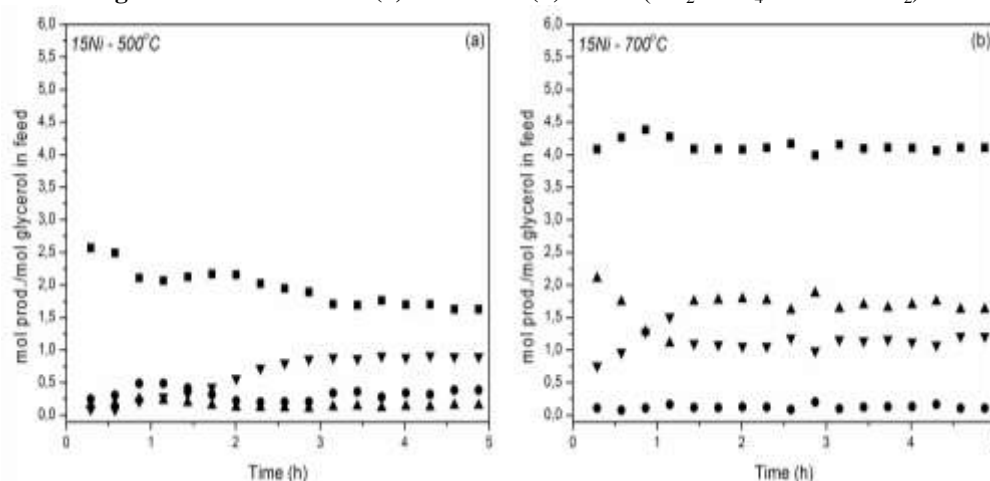


Table 3 shows the results of the 15Ni catalyst GSR for 5h at different temperatures. According to Figure 7, the 15Ni catalysts were stable at both temperatures evaluated.

Table 3. 15Ni C gaseous product yield (mol_{prod}/mol_{glycerol fed}), H₂/CO₂ and CO₂/CO rate (mol/mol), volume of liquid effluent collected (mL), global glycerol conversion (%) in 5-h reaction at 500°C, 600°C and 700°C, and carbon formation (mmol)

15Ni	H ₂	CH ₄	CO	CO ₂	H ₂ /CO ₂	CO ₂ /CO	Effluent	X _{glycerol}	C
500°C	2.4	0.4	0.2	0.8	3.0	4.0	4.9	81	9.5
600°C ^a	4.6	0.5	1.2	1.8	2.6	1.5	3.3	100	6.0
700°C	4.1	0.1	1.7	1.1	3.7	0.6	3.1	100	5.0

^aData based on Table 2

Figure 7. GSR of 15Ni at (a) 500°C and (b) 700°C (■H₂ ●CH₄ ▲CO ▼CO₂)

An increase in the temperature promotes an increase in the glycerol conversion, whereas the liquid effluent volume collected at the end of the reaction decreases (Table 3).

The H₂/CO₂ ratio of the 15Ni catalyst was higher than the theoretical one (2.3mol/mol) at all temperatures studied, therefore, the selectivity in H₂ is higher than the selectivity in CO₂ at all temperatures.

The CO₂/CO ratio was far higher than the theoretical one (1mol/mol) at 500°C, close to the theoretical one at 600°C and below 1 at 700°C. Through the shift reaction (Reaction 3), the CO formed during the steam reforming reaction is converted into CO₂ and H₂. The reaction is reversible and its equilibrium is shifted to the right at lower temperatures. However, at higher temperatures, the reaction equilibrium is shifted to the left, which limits the conversion of CO into CO₂. Therefore, the selectivity of CO increases with increasing temperature.

The temperature range can influence the formation of carbon in steam reforming reactions and the increase in temperature causes a reduction in the carbon deposition during the reaction. Since the Boudouard reaction (Reaction 6) is an exothermic reaction, as the 'shift' reaction (Reaction 3), those reactions are less favored at elevated temperatures. Therefore, the carbon formation from the CO consumption is disfavored at 700°C, which may also explain the higher selectivity in CO at that temperature.

IX. CONCLUSIONS

The amount of Ni in the catalyst affects the selectivity in H₂, CO, CO₂ and CH₄ due to the Ni property of cleaving the C-C bond. Furthermore, 10wt% Ni and 15wt% Ni catalysts showed better performance than the catalyst with 5wt% Ni. An increase in the Ni content in the catalyst promoted a slight increase in the carbon formation during the reaction, which can be associated with the Boudouard reaction favored in the NiO presence.

The 15Ni catalyst was also evaluated for 20h and its behavior was equivalent to that obtained by a 5-hour reaction active throughout the reaction. A scanning electron microscopic analysis conducted in the catalyst after the stability reaction confirmed the formation of filamentous carbon.

The 15Ni catalyst was also tested at 500°C and 700°C and we have concluded temperature is an important factor for the glycerol steam reforming reaction, since some reactions that take place in parallel with glycerol steam reforming are favored or do not depend on temperature. The catalyst shows better performance at 600°C.

ACKNOWLEDGMENTS

The authors acknowledge CAPES, CNPq and FAPESP for the financial support, Electrochemistry Group at IQSC for the XRD analyses and LNLS (Campinas, Brazil) for the in situ XRD and XANES analyses.

REFERENCES

- [1]. Mariño, F.; Baronetti, G.; Jobbagy, M.; Laborde, M. Cu-Ni-K/□-Al₂O₃ supported catalysts for ethanol steam reforming formation of hydrotalcite-type compounds as a result of metal-support interaction. *App. Catal. A. Gen.*, vol. 238, p. 41-54, 2003.
- [2]. Galvita, V.V.; Semin, G.L.; Belyaev, V.D.; Semikolenov, V.A.; Tsiakaras, P.; Sobyanin, V.A. Synthesis gas production by steam reforming of ethanol. *App. Catal. A. Gen.*, vol. 220, p. 123-127, 2001.

- [3]. Thyssen, V.V.; Maia, T.A.; Assaf, E.M. Ni supported on La₂O₃-SiO₂ used to catalyze glycerol steam reforming. *Fuel*, vol. 105, p. 358-363, 2013.
- [4]. Chen, L.F.; Guo, P.J.; Qiao, M.H.; Yan, S.R.; Li, H.X.; Shen, W.; Xu, H.L.; Fan, K.N. Cu/SiO₂ catalysts prepared by the ammonia-evaporation method: Texture, structure, and catalytic performance in hydrogenation of dimethyl oxalate to ethylene glycol. *J. Catal.*, vol. 257, p. 172-180, 2008.
- [5]. Sanchez, E.A.; Comelli, R.A. Hydrogen production by glycerol steam-reforming over nickel and nickel-cobalt impregnated on alumina. *Int. J. Hydrog. Energy*, vol. 39, p. 8650-8655, 2014.
- [6]. Dieuzeide, M.L.; Iannibelli, V.; Jobbagy, M.; Amadeo, N. Steam reforming of glycerol over Ni/Mg/g-Al₂O₃ catalysts. Effect of calcination temperatures. *Int. J. Hydrog. Energy*, vol. 37, p. 14926-14930, 2012.
- [7]. Thyssen, V.V.; Assaf, E.M. Ni/La₂O₃-SiO₂ catalysts applied in glycerol steam reforming reaction : effect of the preparation method and reaction temperature. *J. Braz. Chem. Soc.*, vol. 25, p. 2455-2465, 2014.
- [8]. Farrauto, R.J.; Bartholomew, C.H. *Fundamentals of Industrial Catalytic Processes*, Chapman & Hall, London, 1997.
- [9]. Guo, C.; Zhang, X.; Zhang, J.; Wang, Y. Preparation of La₂NiO₄ catalyst and catalytic performance for partial oxidation of methane. *J. Mol. Catal. A. Chem.*, vol. 269, p. 254-259, 2007.
- [10]. Dieuzeide, M.L.; Jobbagy, M.; Amadeo, N. Glycerol steam reforming over Ni/Mg/□-Al₂O₃ catalysts effect of Ni(II) content. *Int. J. Hydrog. Energy*, vol. 39, p. 16976-16982, 2014.
- [11]. Vita, A.; Pino, L.; Cipiti, F.; Laganà, M.; Recupero, V. Biogas as renewable raw material for syngas production by tri-reforming process over NiCeO₂ catalysts: Optimal operative condition and effect of nickel content. *Fuel Process. Technol.*, vol. 127, p. 47-58, 2014.
- [12]. Wang, C.; Dou, B.; Chen, H.; Song, Y.; Xu, Y.; Du, X.; Zhang, L.; Luo, T.; Tan, C. Renewable hydrogen production from steam reforming of glycerol by Ni-Cu-Al, Ni-Cu-Mg, Ni-Mg catalysts. *Int. J. Hydrog. Energy*, vol. 38, p. 3562-3571, 2013.
- [13]. Li, Z.; Hu, X.; Zhang, L.; Liu, S.; Lu, G. Steam reforming of acetic acid over Ni/ZrO₂ catalysts: Effects of nickel loading and particle size on product distribution and coke formation. *App. Catal. A. Gen.*, vol. 417, p. 281-289, 2012.
- [14]. Seo, Y.S.; Jung, Y.S.; Yoon, W.L.; Jang, I.G.; Lee, T.W. The effect of Ni content on a highly active NiAl₂O₃ catalyst prepared by the homogeneous precipitation method. *Int. J. Hydrog. Energy*, vol. 36, p. 94-102, 2011.
- [15]. Han, S.J.; Bang, Y.; Yoo, J.; Seo, J.G.; Song, I.K. Hydrogen production by steam reforming of ethanol over mesoporous NiAl₂O₃ZeZrO₂ xerogel catalysts: Effect of nickel content. *Int. J. Hydrog. Energy*, vol. 38, p. 8285-8292, 2013.
- [16]. Fierro, V.; Akdim, O.; Provendier, H.; Mirodatos, C. Ethanol oxidative steam reforming over Ni-based catalysts. *J. Power Sources*, vol. 145, p. 659-666, 2005.
- [17]. Trimm, D.L. Catalysis for the control of coking during steam reforming. *Catal. Today*, vol. 49 p. 3-10, 1999.
- [18]. Bradford, M.C.J.; Vannice, M.A. Catalytic reforming of methane with carbon dioxide over nickel catalysts. I. Catalyst characterization and activity. *App. Catal. A. Gen.*, vol. 142, p. 73-96, 1996.
- [19]. Figueiredo, J.L.; Ribeiro, F.R. *Catálise Heterogênea*. Fundação Calouste Gulbenkian, Lisboa, 1989.
- [20]. Lee, W.J.; Li, C.Z. Opposite effects of gas flow rate on the rate of formation of carbon during the pyrolysis of ethane and acetylene on a nickel mesh catalyst. *Carbon*, vol. 46, p. 1208-1217, 2008.
- [21]. Pasetyo, I.; Do, D.D. Pore structure alteration of porous carbon by catalytic coke deposition. *Carbon*, vol. 37, p. 1909-1918, 1999.